Anomalous Hall effect on the surface of topological Kondo insulators

E. J. König, P. M. Ostrovsky, M. Dzero, and A. Levchenko

Phys. Rev. B **94**, 041403 — Published 7 July 2016

DOI: 10.1103/PhysRevB.94.041403

Anomalous Hall Effect on the surface of topological Kondo insulators

E. J. König,[1] P. M. Ostrovsky,[2,3] M. Dzero,[4] and A. Levchenko[1]

[1]*Department of Physics, University of Wisconsin-Madison, Madison, Wisconsin 53706, USA*
[2]*Max Planck Institute for Solid State Research, Heisenbergstr. 1, 70569 Stuttgart, Germany*
[3]*L. D. Landau Institute for Theoretical Physics RAS, 119334 Moscow, Russia*
[4]*Department of Physics, Kent State University, Kent, OH, 44242, USA*

(Dated: April 26, 2016)

We calculate the anomalous Hall conductivity σ_{xy} of the surface states in cubic topological Kondo insulators. We consider a generic model for the surface states with three Dirac cones on the (001) surface. The Fermi velocity, the Fermi momentum and the Zeeman energy in different Dirac pockets may be unequal. The microscopic impurity potential mediates mixed intra and interband extrinsic scattering processes. Our calculation of σ_{xy} is based on the Kubo-Streda diagrammatic approach. It includes diffractive skew scattering contributions originating from the rare two-impurity complexes. Remarkably, these contributions yield anomalous Hall conductivity that is independent of impurity concentration, and thus is of the same order as other known extrinsic side jump and skew scattering terms. We discuss various special cases of our results and the experimental relevance of our study in the context of the recent hysteretic magnetotransport data in SmB_6 samples.

PACS numbers: 72.10.Fk, 72.25.-b, 73.23.-b, 75.20.Hr

Topological Kondo insulators. Topological insulators [1–3] remain a vibrant field of research in present day condensed matter physics. The main thrusts for this extraordinary scientific interest include the vast potential technological applications in the fields of nanoelectronics and quantum computation as well as the fascinating innovative realization of fundamental concepts from quantum field theory and differential geometry.

Among the various realizations of topological phases of matter, topological Kondo insulators (TKIs) [4, 5], take a special place. Their topologically protected metallic surface states emerge as a result of the hybridization between weakly correlated conduction electrons and strongly correlated states. In particular, theories [6–9] describing states on the (001) surface suggest a low energy Hamiltonian with three Dirac bands located at Γ, X and Y points of the surface Brillouin zone (BZ). Main experimentally distinguishing characteristics of the TKIs are the saturation of resistivity at very low temperatures, pronounced temperature dependence of the magnetic susceptibility across a wide range of temperatures and a fairly narrow insulating gap [10, 11]. Intriguing recent experimental evidence for the TKI physics was reported in SmB_6 samples revealing the predicted surface dominated transport directly [12], by thickness independent resistivity measurements [13], and 2D (surface) weak antilocalization data [14]. Furthermore, characteristics of Dirac electrons were revealed using ARPES [15–17] and torque magnetometry [18]. In addition, hysteretic magneto-transport measurements have been reported by several groups [19, 20]. This effect can be attributed to ferromagnetic domains formed on the surface by unscreened samarium magnetic moments or samarium sesquioxide (Sm_2O_3) impurities.

It has been also proposed that the surface states in SmB_6 may be of conventional type [21, 22], i.e. they have quadratic dispersion modified by the presence of strong spin-orbit coupling. Note, that in this scenario, the conduction states will remain decoupled from the Sm moments on the surface via the Kondo breakdown mechanism, so that ferromagnetic ordering of the samarium f-moments would still be possible. This controversy - Dirac vs. conventional surface states - motivates us to study the magneto-transport properties of the surface states on the background of induced non-zero magnetization. Specifically, in this paper we calculate the anomalous Hall conductivity for a cubic topological Kondo in-

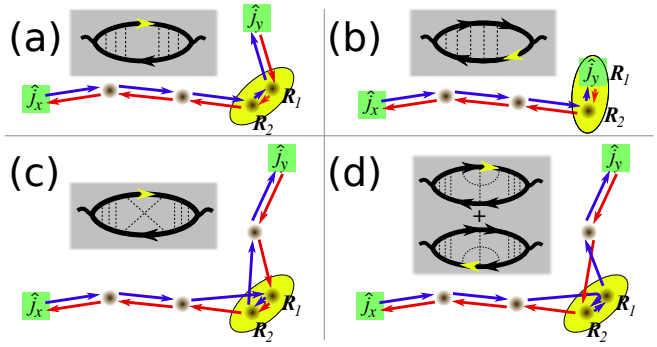

FIG. 1: Diagrammatic representation and real space trajectories for extrinsic contributions to σ_{xy}. Quantum complexes responsible for the AHE are shown by an ellipse with focuses in points $\boldsymbol{R_1}$ and $\boldsymbol{R_2}$. In the non-crossing approximation, both skew-scattering (a) and sidejump (b) contributions rely on coherent interband scattering between opposite branches of the Dirac spectrum. The corresponding virtual states as well as off-shell excitations entering crossed X and Ψ diagrams, (c) and (d) respectively, are marked by a yellow arrow in exemplary positions of the diagrams. Due to the uncertainty principle, the typical extension of a quantum complex is thus of the order of Fermi wavelength $|\boldsymbol{R_1} - \boldsymbol{R_2}| \sim \lambda_F$.

sulator with three Dirac surface bands. Our results for the anomalous Hall conductivity allow us to elucidate experimentally distinguishable characteristics of the Dirac electrons and should help to resolve the controversy discussed above.

Anomalous Hall effect. Electron transport in ferromagnets has a long history going back to E. Hall's 1881 discovery of the anomalous Hall effect (AHE) [23], i.e. of a transverse conductivity σ_{xy} generated by the magnetization (Zeeman coupling) rather than by orbital coupling to a magnetic field. To account for this effect, two equally appropriate techniques are commonly employed. First, in the semiclassical approach [24] different terms in σ_{xy} stem from distinct physical mechanisms of intrinsic [25], skew scattering [26] and side jump [27] contributions. Second, σ_{xy} can be directly calculated using Kubo-Streda diagrammatic response theory [28]. Semiclassics appear to be more intuitive, while the diagrammatic treatment is more systematic. Notably, an additional skew scattering mechanism was discovered only very recently with the help of diagrams [29–31]. Physically, it originates from *diffractive skew scattering* off two impurities residing about one Fermi wavelength λ_F from each other. Diagrammatically, these processes can be understood by considering crossed impurity lines in the conductivity bubble [see Fig. 1 (c,d)], and can be equivalently treated in the semiclassical approach provided that crossed impurity lines are included into the full scattering amplitude. At first glance, this observation seems to be in sharp contrast with conventional wisdom of the impurity diagrammatic technique [32] that dictates that a single cross of impurity lines implies a rare disorder configuration and thus smallness in the parameter $\lambda_F/l \ll 1$, where l is the elastic mean free path. However, it should be stressed that even previously discussed [24–27, 29, 33] contributions of weak impurities to the AHE rely on rare impurity configurations (see Fig. 1). Therefore, both crossed and non-crossed diagrams are of the same order and suppressed by λ_F/l as compared to the diagonal conductance. Diagrams with more than a single cross are even smaller [34]. These qualitative arguments are fully supported by the microscopic computation which we present in the remainder of the paper.

To make the diffractive analogy transparent we present in Fig. 1 examplary electron trajectories in real space. The probability $p_{AB} = |\sum_i A_i|^2 = \sum_{ij} A_i A_j^*$ of reaching a point $\boldsymbol{r}_B$ from $\boldsymbol{r}_A$ is the square of the sum of the amplitudes for all paths i, j. In Fig. 1, A_i and A_j^* are represented by different colors and opposite orientation of arrows. In the non-crossing approximation, $p_{AB}^{(nc)} = \sum_i |A_i|^2$, and all interference terms are omitted. The crossed X-diagrams contribute $p_{AB}^X = \sum'_{i\neq j} A_i A_j^*$, where the sum includes pairs of non-equal trajectories equivalent to Fig. 1 (c). An analogous expression holds for p_{AB}^Ψ. The interference pattern becomes apparent in the plots of spatially-resolved scattering probabilities

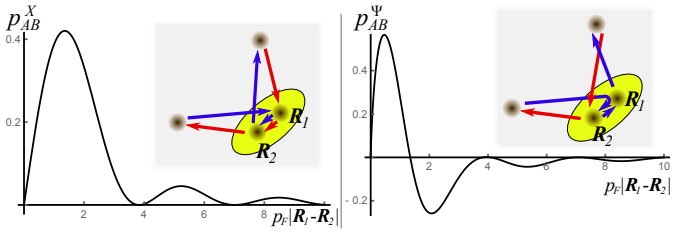

FIG. 2: Diffractive skew scattering: Spatially-resolved scattering probabilities p_{AB}^X and p_{AB}^Ψ for intraband scattering.

$p_{AB}^{X,\Psi}$ off two-impurity complexes, see Fig. 2. The latter exhibit pronounced Fraunhofer oscillatory interference patterns. The novel extrinsic contributions [Fig. 1 (c,d)] constitute inherent parts of the skew scattering and should necessarily be included to properly compute the transverse conductivity. These terms can be distinguished from previously studied processes [Fig. 1 (a,b)] by means of their diffractive nature.

Model and Assumptions. We employ the diagrammatic approach to calculate the anomalous Hall response on the surface of 3D TKIs with cubic symmetry taking into account all the diagrams to the leading order in impurity concentration. For this purpose, consider the following low energy Hamiltonian

$$\underline{H}_0 = \sum_K \left[v_K \boldsymbol{\sigma} \cdot \boldsymbol{p} + m_K \sigma_z + E_K \right] \underline{\Pi}_K. \qquad (1)$$

Throughout the paper, matrices in the space of Dirac pockets (DPs) are denoted by an underscore and have indices $K, K' \in \{\Gamma, X, Y\}$. The symbol $\underline{\Pi}_K$ denotes a projector on Kth DP. Rotational C_4 symmetry imposes $v_X = v_Y \equiv v$, $m_X = m_Y \equiv m$. We count energies from the Dirac point of the X pocket, $E_X = E_Y \equiv 0$, and momenta in X (Y) pocket relative to $\boldsymbol{Q}_{X(Y)} = (\pi/a)\hat{\boldsymbol{e}}_{X(Y)}$ (a is the lattice spacing). For simplicity we omit the anisotropy of X and Y pockets and set $\hbar = 1$ in the intermediate formulas (we restore Planck's constants in the final expressions for σ_{xy}). The Hamiltonian in Eq. (1) contains just two essential ingredients for the finite AHE, namely spin-orbit coupling and time reversal symmetry breaking, which is implicit in the mass term of the Dirac fermions.

Our model also contains uniformly distributed scalar impurities with isotropic potential $u(|\boldsymbol{r}|)$ which is short-ranged on the scale of the smallest Fermi wavelength $\min_K(p_{F,K}^{-1})$ with $v_K p_{F,K} = \sqrt{\epsilon_K^2 - m_K^2}$ where $\epsilon_K = \epsilon - E_K$ and ϵ is the Fermi energy. Our calculation is controlled in the parameter $n_{\rm imp}/n_{\rm min} \ll 1$ with $n_{\rm imp}$ and $n_{\rm min} = \min_K(n_K)$ being the impurity concentration and the carrier density of the least populated pocket respectively. We assume weak impurities and treat them in the leading Born approximation.

Technically, the anomalous Hall response involves virtual states (off-shell contributions) residing within the

radius $\Delta p = 3\max_K(p_{F,K})$ around Γ, X, Y and M points of the BZ. As a consequence, the minimal three-band model Eq. (1) is applicable only for sufficiently small Fermi momenta $\max_K(p_{F,K}) \ll \pi/a$. Furthermore, the contribution to σ_{xy} originating from the states in the vicinity of the M point is negligible provided $\sqrt{2m_M\Delta} \gg \min_K(p_{F,K})$, where m_M (Δ) is the effective mass (excitation gap of closest states) at the M point [35].

Results. We now turn our attention to the Hall response. Here we present our main results and delegate the details on the calculations to the Supplementary Materials. When the Fermi energy lies in the gap, $|\epsilon_K| < |m_K|$, the contribution of the Kth DP to the Hall response stems from the intrinsic mechanism, so called *anomalous velocity* contribution to AHE, as originally introduced by Karplus and Luttinger [25]. Its topological origin was realized much later [38], and can be equivalently understood in terms of the Berry curvature that acts as an effective magnetic field for electron wave-packet motion in parameter space of momenta. Indeed, the Hall conductivity can be presented as $\sigma_{xy}|_K = -(e^2v_K^2/2\pi h)\int\Omega_{xy}(k)d^2k$, where the Berry curvature for a single gapped Dirac cone is given explicitly by $\Omega_{xy}(k) = m_K/2(m_K^2 + v_K^2k^2)^{3/2}$ so that upon momentum integration we find $\sigma_{xy}|_K = -(\mathrm{sgn}(m_K)/2)(e^2/h)$. The half-integer quantization is a consequence of fermion number fractionalization [35–37].

In contrast, outside the gap the σ_{xy} is not quantized. We switch to a matrix representation in DP space and find

$$\sigma_{xy} = 2\frac{e^2}{h}\underline{\boldsymbol{v}}\underline{F}\left[\underline{b} + \underline{a}[\underline{x} + \underline{\psi}]\underline{a}\right]\underline{F}^T\underline{\boldsymbol{v}}^T. \tag{2}$$

In this expression, the bare velocity vertex is $\underline{\boldsymbol{v}} = (v_\Gamma, v, v)$ and the trace over spin space was already performed. The various contributions have the following origin [cf. Fig. 1]: $\underline{F}$ is the noncrossed vertex correction, in which at each stringer $\underline{a}$ of the ladder only contributions which are on-shell were kept; $\underline{b}$ is also part of the ladder in diagram, but involves contributions away from the Fermi surface; finally $\underline{x}$ [$\underline{\psi}$] originates from the central part of diagram (c) [diagram (d)]. All the elements of Eq. (2) are derived explicitly in Ref. [35] in terms of the microscopic parameters of the model. The anomalous Hall response, Eqs. (2), constitutes the main result of our work. Unlike previous calculations of the AHE in multiband systems [39, 40], we included diagrams with crossed impurity lines as they equally contribute to the leading order approximation. The common physical origin of crossed diagrams manifests itself in the complementary contributions from the off-diagonal terms in $\underline{x}_{KK'}$ and $\underline{\psi}_{KK'}$.

Discussion. We now analyze our general result for the anomalous Hall response, Eqs. (2), in various simplifying cases. We consider both particular limits of the impurity potential $u(\boldsymbol{r})$, and special values of the parameters entering the clean Hamiltonian (1).

(i) Smooth disorder potential. We first consider the case when $u(\boldsymbol{r})$ is smooth on the scale of the lattice constant a. Interband scattering is negligible and we obtain

$$\sigma_{xy} = \sigma_{xy}^{(0)}(|\epsilon_\Gamma|/m_\Gamma) + 2\sigma_{xy}^{(0)}(|\epsilon|/m). \tag{3}$$

The anomalous Hall conductivity of a single Dirac cone is [30]

$$\sigma_{xy}^{(0)}\left(\frac{|\epsilon|}{m}\right) = -\frac{e^2}{2h}\left[\frac{16|\epsilon|m^3\theta(\epsilon^2-m^2)}{(\epsilon^2+3m^2)^2} + \theta(m^2-\epsilon^2)\right]. \tag{4}$$

It should be noted that in this case there is no contribution from the Ψ skew scattering diagrams [see Fig. 1 (d)] as they vanish. This pecularity is accidental and specific to the single Dirac cone limit. It can be traced back to the destructive interference of scattering from two-impurity complexes as evidenced from the plot of the probability p_{AB}^{Ψ} in Fig. 2. The result for smooth disorder potential is plotted in Fig. 3 using dotted curves.

(ii) Fermi momentum in the gap. In what follows we restore the possibility of nonzero interpocket scattering. When $\epsilon^2 < m^2$, i.e. when the Fermi energy is in the gap of X and Y pockets, the problem essentially simplifies to a single Dirac cone and Eq. (3) holds again (using $2\sigma_{xy}^{(0)}(|\epsilon|/m) = -e^2/h$).

Further, when $\epsilon_\Gamma^2 < m_\Gamma^2$ (Fermi energy in the gap of the Γ pocket) the problem simplifies to two equal Dirac cones. Surprisingly, the resulting Hall conductivity is again given by Eq. (3) (using $\sigma_{xy}^{(0)}(|\epsilon_\Gamma|/m_\Gamma) = -e^2/2h$) and is independent on the range of $u(\boldsymbol{r})$.

(iii) Equal DPs. We next consider the situation when the three DPs are equal, i.e. $E_\Gamma = 0$, $v_\Gamma = v$ and $m_\Gamma = m$. The general expression for the Hall conductance is presented in Ref. [35]. We note that for smooth disorder potential, the effect of intraband scattering enters only to second order ($\epsilon^2 > m^2$)

$$\sigma_{xy} = \sigma_{xy}^{(0)}\left(\frac{|\epsilon|}{m}\right)\left[3 + \left(\frac{\epsilon^2}{m^2} - 1\right)\frac{W_{\Gamma X}^2 + 2W_{\Gamma X}W_{XY}}{W^2}\right]. \tag{5}$$

Here, $W = n_{\mathrm{imp}}|\tilde{u}(0)|^2$, $W_{\Gamma X} = n_{\mathrm{imp}}|\tilde{u}(\pi/a)|^2$, and $W_{XY} = n_{\mathrm{imp}}|\tilde{u}(\sqrt{2}\pi/a)|^2$, where $\tilde{u}(\boldsymbol{q})$ is the Fourier transform of $u(\boldsymbol{r})$. While the single band Hall conductivity, Eq. (4), decays as $|\epsilon|^{-3}$, for finite $W_{\Gamma X}$ we find a term which decays only as $|\epsilon|^{-1}$. Thus interband scattering strongly enhances anomalous Hall conductivity. This effect persists to the case of arbitrary interband scattering. The Hall conductance (5) continuously approaches the gap value $\sigma_{xy} = -3\mathrm{sgn}(m)e^2/2h$.

(iv) Point like scatterers. When the impurity potential is short ranged on the scale of a, the matrix $\underline{W}_{K,K'} = n_{\mathrm{imp}}|u(0)|^2$ for all K, K'. The experimental analysis of the weak-antilocalization effect [41] in SmB_6 samples [14, 20] suggests that this limit is most important for present day experiments.

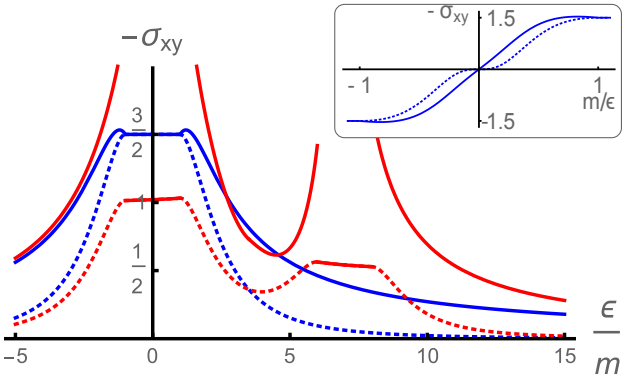

FIG. 3: Comparison of the AHE in the cases of a smooth disorder potential (dotted) and point like scatterers (solid). We assumed $m_\Gamma = m$ and additionally imposed $v_\Gamma = v$ in the case of short ranged impurities. For the blue curves, we set $\epsilon_\Gamma = \epsilon$ while the red curves are obtained for $\epsilon_\Gamma = \epsilon - 7m$. Main panel: plot of σ_{xy} as a function of ϵ/m assuming $m > 0$. Inset: the same quantity for $\epsilon_\Gamma = \epsilon$ as a function of the inverse parameter.

The explicit formula of $\sigma_{xy}(\epsilon/m, \epsilon_\Gamma/m)$ for the case $v_\Gamma = v$, and $m_\Gamma = m$ has been relegated to Ref. [35]. If $\epsilon_\Gamma = \epsilon$ this result further simplifies to

$$\sigma_{xy} = -\frac{e^2}{h}\frac{8|\epsilon|m\left(\epsilon^2+8m^2\right)}{3\left(\epsilon^2+3m^2\right)^2}. \tag{6}$$

A graphical comparison between the cases of smooth disorder and point like impurities is shown in Fig. 3. It should be noted, that in the limit of short range scatters our result for the Hall conductance ceases to be a continuous function: it displays discontinuities at $\epsilon_K = m_K$. A similar behavior was recently found in the Bychkov-Rashba model [31]. This is an artifact of an approximation that exploits the basic assumption $n_{\rm imp} \ll n_{\rm min}$. As a consequence, our result is not applicable in the energy window where $|\epsilon_K - m_K|$ is smaller than the elastic scattering rate. A more elaborate calculation should reveal smoothening of the discontinuities in the immediate vicinity of the band edges.

Conclusion and outlook. Experimental and theoretical studies of the Hall effect in f-orbital materials remain a very active area of research for several decades [52]. In the heavy fermion metallic state, the f-electrons in the bulk are a primary source of the skew-scattering contribution to the anomalous Hall effect. In contrast, we here considered an ideal topological Kondo insulator, in which bulk states do not contribute to transport. With the advent of SmB_6 as a prominent candidate for a strongly correlated topological insulator, it was immediately realized that at sufficiently low temperatures the Hall conductivity should be surface dominated. In fact, Kim et al. [13] have demonstrated thickness-independent surface Hall effect below $T \approx 5$ K, which suggests that our results can be tested experimentally.

Inasmuch experiments on TKIs are concerned, our most important conclusion is that the magnetization and gate voltage dependence of the AHE can be used to gain information about the microscopic nature of surface states and impurities. Indeed, the analysis of various limiting cases of the three-band Dirac model reveals that the large energy asymptote of the anomalous Hall response scales as $(m/|\epsilon|)^3$ in the case of smooth impurity potential while $\sigma_{xy} \sim m/|\epsilon|$ for short range scatterers. This behavior persists in the generic result. In contrast, in the Bychkov-Rashba model [31], $\sigma_{xy} \propto m/\epsilon^2$.

As mentioned in the introduction, present day experimental samples are believed to host a multitude of large ferromagnetic domains. In our theory, smooth fluctuations of the magnetization can be taken into account by averaging the final result. Even after this procedure, the asymptotics allow to distinguish smooth and sharp impurity potentials in the described manner. Up to now magnetotransport experiments on TKIs concentrated a hysteretic behavior in the longitudinal conductance. Systematic investigation of the transverse conductance is still needed.

In conclusion, we presented a theory for the anomalous Hall response on the surface of a cubic topological Kondo insulator with three Dirac valleys allowing for unequal Fermi and Zeeman energies as well as unequal Fermi velocities. Specifically, we analyzed the semiclassical AHE and uncovered the importance of diffractive skew scattering in the context of topological Kondo insulators. In a parallel vein, our results have further rich consequences for anomalous transport phenomena in other multiband material systems such as Weyl semimetals [42] and chiral p-wave superconductors [43–45]. Quantum effects, such as interaction and localization corrections to the conductivity tensor, the quantum AHE [46–48] and the surface state quantum Hall effect [37, 49–51] on TKIs remain a theoretical and experimental challenge for the future. One important issue of the possible effects of magnetic scattering on anomalous Hall conductivity in SmB_6 we leave for a separate publication. Lastly, as a byproduct of this analysis, we found that a system of two equal Dirac cones (as it occurs in graphene) displays an AHE which is universal and independent of details of the scattering potential.

Acknowledgements. We thank A. Andreev, I. Dmitriev, M. Khodas, L. Li, J. Sauls, K. Sun and M. Titov for important discussions and acknowledge hospitality by the Department of Physics and Astronomy at Michigan State University (A.L., P.M.O. and E.J.K.) and by the Department of Physics at University of Michigan (E.J.K.). This work was financially supported in part by NSF Grant No. DMR-1506547 (M.D.), and NSF Grant No. DMR-1606517 (E.J.K. and A.L.). Support for this research at the University of Wisconsin-Madison was provided by the Office of the Vice Chancellor for Research and Graduate Education with funding from

the Wisconsin Alumni Research Foundation.

[1] M. Z. Hasan and C. L. Kane, Rev. Mod. Phys. **82**, 3045 (2010).
[2] X.-L. Qi and S.-C. Zhang, Rev. Mod. Phys. **83**, 1057 (2011).
[3] B. Bernevig and T. Hughes, *Topological Insulators and Topological Superconductors* (Princeton University Press, 2013), ISBN 9780691151755.
[4] M. Dzero, K. Sun, V. Galitski, and P. Coleman, Phys. Rev. Lett. **104**, 106408 (2010).
[5] M. Dzero, J. Xia, V. Galitski, and P. Coleman, preprint arXiv:1506.05635 (2015).
[6] F. Lu, J. Zhao, H. Weng, Z. Fang, and X. Dai, Phys. Rev. Lett. **110**, 096401 (2013).
[7] V. Alexandrov, M. Dzero, and P. Coleman, Phys. Rev. Lett. **111**, 226403 (2013).
[8] M. Ye, J. Allen, and K. Sun, preprint arXiv:1307.7191 (2013).
[9] B. Roy, J. D. Sau, M. Dzero, and V. Galitski, Phys. Rev. B **90**, 155314 (2014).
[10] A. Menth, E. Buehler, and T. H. Geballe, Phys. Rev. Lett. **22**, 295 (1969).
[11] J. W. Allen, B. Batlogg, and P. Wachter, Phys. Rev. B **20**, 4807 (1979).
[12] S. Wolgast, C. Kurdak, K. Sun, J. W. Allen, D.-J. Kim, and Z. Fisk, Phys. Rev. B **88**, 180405 (2013).
[13] D. J. Kim, S. Thomas, T. Grant, J. Botimer, Z. Fisk, and J. Xia, Scientific Rep. **3**, 3150 EP (2013).
[14] S. Thomas, D. Kim, S. Chung, T. Grant, Z. Fisk, and X. J. (2013), arXiv1307.4133.
[15] M. Neupane, N. Alidoust, S. Xu, T. Kondo, Y. Ishida, D.-J. Kim, C. Liu, I. Belopolski, Y. Jo, T.-R. Chang, et al., Nat. Comm. **4** (2013).
[16] N. Xu, X. Shi, P. K. Biswas, C. E. Matt, R. S. Dhaka, Y. Huang, N. C. Plumb, M. Radović, J. H. Dil, E. Pomjakushina, et al., Phys. Rev. B **88**, 121102 (2013).
[17] J. Jiang, S. Li, T. Zhang, Z. Sun, F. Chen, Z. Ye, M. Xu, Q. Ge, S. Tan, X. Niu, et al., Nat. Comm. **4** (2013).
[18] G. Li, Z. Xiang, F. Yu, T. Asaba, B. Lawson, P. Cai, C. Tinsman, A. Berkley, S. Wolgast, Y. S. Eo, et al., Science **346**, 1208 (2014).
[19] S. Wolgast, Y. S. Eo, T. Öztürk, G. Li, Z. Xiang, C. Tinsman, T. Asaba, B. Lawson, F. Yu, J. W. Allen, K. Sun, L. Li, Ç. Kurdak, D.-J. Kim, and Z. Fisk, Phys. Rev. B **92**, 115110 (2015).
[20] Y. Nakajima, P. S. Syers, X. Wang, R. Wang, and J. Paglione, preprint arXiv:1312.6132 (2013).
[21] Z.-H. Zhu, A. Nicolaou, G. Levy, N. P. Butch, P. Syers, X. F. Wang, J. Paglione, G. A. Sawatzky, I. S. Elfimov, and A. Damascelli Phys. Rev. Lett. **111**, 216402 (2013).
[22] P. Hlawenka, K. Siemensmeyer, E. Weschke, A. Varykhalov, J. Snchez-Barriga, N. Y. Shitsevalova, A. V. Dukhnenko, V. B. Filipov, S. Gabni, K. Flachbart, O. Rader, E. D. L. Rienks, preprint arXiv:1502.01542 (2015).
[23] N. Nagaosa, J. Sinova, S. Onoda, A. MacDonald, and N. Ong, Rev. Mod. Phys. **82**, 1539 (2010).
[24] N. A. Sinitsyn, J. of Phys.: Cond. Matt. **20**, 023201 (2008).
[25] R. Karplus and J. M. Luttinger, Phys. Rev. **95**, 1154 (1954).
[26] J. Smit, Physica **21**, 877 (1955).
[27] L. Berger, Physica **30**, 1141 (1964).
[28] P. Streda, J. Phys. C **15**, L717 (1982).
[29] N. Sinitsyn, A. MacDonald, T. Jungwirth, V. Dugaev, and J. Sinova, Phys. Rev. B **75**, 045315 (2007).
[30] I. A. Ado, I. A. Dmitriev, P. M. Ostrovsky, and M. Titov, Europhys. Lett. **111**, 37004 (2015).
[31] I. A. Ado, I. A. Dmitriev, P. M. Ostrovsky, and M. Titov, preprint arXiv:1511.07413 (2015).
[32] A. A. Abrikosov, L.P. Gor'kov, and I. E. Dzyaloshinskii, *Quantum Field Theoretical Methods in Statistical Physics*, (Pergamon, 1965).
[33] N. A. Sinitsyn, J. E. Hill, H. Min, J. Sinova, and A. H. MacDonald, Phys. Rev. Lett. **97**, 106804 (2006).
[34] Maximally crossed diagrams can form an exception, since they lead to interference corrections.
[35] Supplementary materials to this article.
[36] R. Jackiw and C. Rebbi, Phys. Rev. D **13**, 3398 (1976).
[37] E. König, P. Ostrovsky, I. Protopopov, I. Gornyi, I. Burmistrov, and A. Mirlin, Phys. Rev. B **90**, 165435 (2014).
[38] Ming-Che Chang and Qian Niu, Phys. Rev. Lett. **75**, 1348 (1995).
[39] A. A. Kovalev, Y. Tserkovnyak, K. Vỳbornỳ, and J. Sinova, Phys. Rev. B **79**, 195129 (2009).
[40] A. A. Kovalev, J. Sinova, and Y. Tserkovnyak, Phys. Rev. Lett. **105**, 036601 (2010).
[41] M. Dzero, M. G. Vavilov, K. Kechedzhi, and V. Galitski, Phys. Rev. B **92**, 165415 (2015).
[42] A. A. Burkov, Phys. Rev. Lett. **113**, 187202 (2014).
[43] Roman M. Lutchyn, Pavel Nagornykh, Victor M. Yakovenko, Phys. Rev. B **80**, 104508 (2009).
[44] E. Tailor, C. Kallin, Phys. Rev. Lett. **108**, 157001 (2012).
[45] Songci Li, A. V. Andreev, B. Z. Spivak, Phys. Rev. B **92**, 100506 (2015).
[46] H. Weng, R. Yu, X. Hu, X. Dai, and Z. Fang, Adv. in Phys. **64**, 227 (2015).
[47] C.-X. Liu, S.-C. Zhang, and X.-L. Qi, preprint arXiv:1508.07106 (2015).
[48] C.-Z. Chang and M. Li, preprint arXiv:1510.01754.
[49] X.-L. Qi, R. Li, J. Zang, and S.-C. Zhang, Science **323**, 1184 (2009).
[50] C. Brüne, C. X. Liu, E. G. Novik, E. M. Hankiewicz, H. Buhmann, Y. L. Chen, X. L. Qi, Z. X. Shen, S. C. Zhang, and L. W. Molenkamp, Phys. Rev. Lett. **106**, 126803 (2011).
[51] R. Yoshimi, A. Tsukazaki, Y. Kozuka, J. Falson, K. S. Takahashi, J. G. Checkelsky, N. Nagaosa, M. Kawasaki, and Y. Tokura, Nat. Comm. **6** (2015).
[52] S. Nair, S. Wirth, S. Friedemann, F. Steglich, Q. Si and A. J. Schofield, Advances in Physics **61**, 583 (2012).